Dispersion tailoring and compensation by modal interactions in OmniGuide fibers

Torkel D. Engeness, Mihai Ibanescu, Steven G. Johnson, Ori Weisberg, Maksim Skorobogatiy, Steven Jacobs, and Yoel Fink

OmniGuide Communications, One Kendall Sq. building 100, 3rd floor, Cambridge, Massachusetts 02139

torkel@omni-guide.com

Abstract: We present a method for dispersion-tailoring of OmniGuide and other photonic band-gap guided fibers based on weak interactions ("anticrossings") between the core-guided mode and a mode localized in an intentionally introduced defect of the crystal. Because the core mode can be guided in air and the defect mode in a much higher-index material, we are able to obtain dispersion parameters in excess of 500,000 ps/nm-km. Furthermore, because the dispersion is controlled entirely by geometric parameters and not by material dispersion, it is easily tunable by structural choices and fiber-drawing speed. So, for example, we demonstrate how the large dispersion can be made to coincide with a dispersion slope that matches commercial silica fibers to better than 1%, promising efficient compensation. Other parameters are shown to yield dispersion-free transmission in a hollow OmniGuide fiber that also maintains low losses and negligible nonlinearities, with a nondegenerate TE_{01} mode immune to polarization-mode dispersion (PMD). We present theoretical calculations for a chalcogenide-based material system that has recently been experimentally drawn.

OCIS codes: (060) Fiber optics and optical communications (060.2340) Fiber optics components (230) Optical devices (230.1480) Bragg reflectors

References and links

1. S. G. Johnson, M. Ibanescu, M. Skorobogatiy, O. Weisberg, T. D. Engeness, M. Soljačić, S. A. Jacobs, J. D. Joannopoulos, and Y. Fink, "Low-loss asymptotically single-mode propagation in large-core OmniGuide fibers," Opt. Express **9,** 748–779 (2001), http://www.opticsexpress.org/abstract.cfm?URI=OPEX-9-13-748
2. P. Yeh, A. Yariv, and E. Marom, "Theory of Bragg fiber," J. Opt. Soc. Am. **68,** 1196–1201 (1978).
3. Y. Fink, J. N. Winn, S. Fan, C. Chen, J. Michel, J. D. Joannopoulos, and E. L. Thomas, "A dielectric omnidirectional reflector," Science **282,** 1679–1682 (1998).
4. J. A. Harrington, "A review of IR transmitting, hollow waveguides," Fiber Integr. Opt. **19,** 211–227 (2000).
5. A. Ferrando, E. Silvestre, P. Andrés, J. J. Miret and M. V. Andrés "Designing the properties of dispersion-flattened photonic crystal fibers," Opt. Express **9,** 687–697 (2001), http://www.opticsexpress.org/abstract.cfm?URI=OPEX-9-13-687
6. J. Marcou, F. Brechet, and P. Roy, "Design of weakly guiding Bragg fibres for chromatic dispersion shifting towards short wavelengths," J. Opt. A: Pure Appl. Opt. **3,** S144–S153 (2001).
7. G. Ouyang, Y. Xu, and A. Yariv, "Theoretical study on dispersion compensation in air-core Bragg fibers," Opt. Express **10,** 899–908 (2002), http://www.opticsexpress.org/abstract.cfm?URI=OPEX-10-17-899
8. M. Notomi, K. Yamada, A. Shinya, J. Takahashi, C. Takahashi, and I. Yokohama, "Extremely large group-velocity dispersion of line-defect waveguides in photonic crystals," Phys. Rev. Lett. **87,** 253902 (2001).
9. T. A. Birks, D. Mogilevstev, J. Knight, and P. S. Russell, "Dispersion compensation using single-material fibers," IEEE Phot. Techn. Lett. **11,** 674–676 (1999).

#2267 - $15.00 US Received March 24, 2003; Revised April 25, 2003

10. S. O. Konorov, A. B. Fedotov, O. A. Kolevatova, E. A. Serebryannikov, D. A. Sidorov-Biryukov, J. M. Mikhailova, A. N. Naumov, V. I. Beloglazov, N. B. Skibina, L. A. Melnikov, A. V. Shcherbakov and A. M. Zheltikov "Waveguide modes and dispersion properties of hollow-core photonic-crystal and aperiodic-cladding fibers," Laser Physics **13,** 148–160 (2003).
11. Y. Fink, D. J. Ripin, S. Fan, C. Chen, J. D. Joannopoulos, and E. L. Thomas, "Guiding optical light in air using an all-dielectric structure," J. Lightwave Tech. **17,** 2039–2041 (1999).
12. S. D. Hart, G. R. Maskaly, B. Temelkuran, P. H. Prideaux, J. D. Joannopoulos, and Y. Fink, "External reflection from omnidirectional dielectric mirror fibers," Science **296,** 510–513 (2002).
13. B. Temelkuran, S. D. Hart, G. Benoit, J. D. Joannopoulos, and Y. Fink, "Wavelength-scalable hollow optical fibres with large photonic bandgaps for CO2 laser transmission," Nature **420,** 650–653 (2002).
14. J. D. Joannopoulos, R. D. Meade, and J. N. Winn, *Photonic Crystals: Molding the Flow of Light* (Princeton U. Press, Princeton, N.J., 1995).
15. P. Yeh, *Optical Waves in Layered Media* (Wiley, New York, 1988).
16. R. Ramaswami and K. N. Sivarajan, *Optical Networks: A Practical Perspective* (Academic, London, 1998).
17. L. G. Cohen, C. Lin, and W. G. French, "Tailoring zero chromatic dispersion into the 1.5-1.6 mu-m low-loss spectral region of single mode fibers," Electron. Lett. **15,** 334–335 (1979).
18. C. Lin, H. Kogelnik, and L. G. Cohen, "Optical-pulse equalization of low-dispersion transmission in single-mode fibers in the 1.3-1.7-mu-m spectral region," Opt. Lett. **5,** 476–478 (1980).
19. A. W. Snyder and J. D. Love, *Optical Waveguide Theory* (Chapman and Hall, London, 1983).
20. S. G. Johnson and J. D. Joannopoulos, "Block-iterative frequency-domain methods for Maxwell's equations in a planewave basis," Opt. Express **8,** 173–190 (2001), http://www.opticsexpress.org/abstract.cfm?URI=OPEX-8-3-173
21. M. Skorobogatiy, M. Ibanescu, S. G. Johnson, O. Weisberg, T. D. Engeness, M. Soljačić, S. A. Jacobs, and Y. Fink, "Analysis of general geometric scaling perturbations in a transmitting waveguide. The fundamental connection between polarization mode dispersion and group-velocity dispersion," J. Opt. Soc. B **19,** 2867–2875 (2002).
22. S. G. Johnson, M. Ibanescu, M. Skorobogatiy, O. Weisberg, J. D. Joannopoulos, and Y. Fink, "Perturbation theory for Maxwell's equations with shifting material boundaries," Phys. Rev. E **65,** 066611 (2002).
23. M. Skorobogatiy, S. A. Jacobs, S. G. Johnson, and Y. Fink, "Geometric variations in high index-contrast waveguides, coupled mode theory in curvilinear coordinates," Opt. Express **10,** 1227–1243 (2002), http://www.opticsexpress.org/abstract.cfm?URI=OPEX-10-21-1227
24. M. Miyagi and S. Kawakami, "Design theory of dielectric-coated circular metallic waveguides for infrared transmission," J. Lightwave Tech. **2,** 116–126 (1984).
25. D. Gloge, "Weakly guiding fibers," Appl. Opt. **10,** 2252-2258 (1971).
26. M. Ibanescu, S. G. Johnson, M. Soljačić, J. D. Joannopoulos, Y. Fink, O. Weisberg, T. D. Engeness, S. A. Jacobs, and M. Skorobogatiy, "Analysis of mode structure in OmniGuide fibers," Phys. Rev. E **67,** 046608, (2003).
27. N. W. Ashcroft and N. D. Mermin, *Solid State Physics* (Holt Saunders, Philadelphia, 1976).
28. H. Haus and W.-P. Huang, "Coupled-mode theory," Proc. IEEE **79,** 1505–1518 (1991).
29. W.-P. Huang, "Coupled-mode theory for optical waveguides: an overview," JOSA A **11,** 963–983 (1994).
30. R. Kashyap, *Fiber Bragg Gratings* (Academic, San Diego, Calif., 1999).
31. K. Thyagarajan, R. K. Varshney, P. Palai, A. K. Ghatak, and I. C. Goyal, "A novel design of a dispersion compensating Fiber," IEEE Phot. Techn. Lett. **8,** 1510–1512 (1996).
32. D. Moss, L. Lunardi, M. Lamont, G. Randall, and P. Colbourne, "Tunable dispersion compensation at 10 Gb/s and 40 Gb/s using multicavity all-pass etalons," in *Optical Fiber Communication Conference* (Optical Society of America, Washington, D.C., 2003), Vol. 1, paper TuD1.
33. L.M. Lundardi, D.J. Moss, S. Chandrasekhar, L.L. Buhl, M. Lamont, S. McLaughlin, G. Randall, P. Colbourne, S. Kiran, and C.A. Hulse, "Tunable dispersion compensation at 40 Gb/s using a multicavity etalon all-pass filter with NRZ, RZ and CS-RZ modulation," J. Lightwave Tech. **20,** 2136–2144 (2002).
34. J. L. Auguste, R. Jindal, J. M. Blondy, M. Clapeau, J. Marcou, B. Dussardier, G. Monnom, D. B. Ostrowsky, B. P. Pal, and K. Thyagarajan, "-1800ps/(nm-km) chromatic dispersion at 1.55μm in dual concentric core fibre," El. Lett. **36,** 1689–1691 (2000).
35. T. Kato, Y. Koyano, and M. Nishimura, "Temperature dependence of chromatic dispersion in various types of optical fiber," Opt. Lett. **25,** 1156–1158 (2000).
36. J. K. Chandalia, B. J. Eggleton, R. S. Windeler, S. G. Kosinski, X. Lu, and C. Xu, "Adiabatic coupling in tapered air-silica microstructured optical fiber," IEEE Phot. Tech. Lett. **13,** 52–54 (2001).
37. B. Z. Katsenelenbaum, L. Mercader del Río, M. Pereyaslavets, M. Sorolla Ayza, and M. Thumm, *Theory of Nonuniform Waveguides: The Cross-Section Method* (Inst. of Electrical Engineers, London, 1998).
38. M. Skorobogatiy, C. Anastassiou, O. Weisberg, T. D. Engeness, S. G. Johnson, S. A. Jacobs, and Y. Fink, submitted to J. Lighwave Technol.
39. T. Kanamori, Y. Terunuma, S. Takahashi, and T. Miyashita, "Chalcogenide glass-fibers for mid-infrared transmission," J. Lightwave Tech. **2,** 607–613 (1984).

#2267 - $15.00 US Received March 24, 2003; Revised April 25, 2003

1. Introduction

1.1. Overview

OmniGuide fiber [1] is a new class of Bragg fiber [2] based on omnidirectional reflectivity [3]. In these fibers, as depicted in Fig. 1(a), a large, hollow core is surrounded by a multilayer omnidirectional mirror that confines light similarly to a hollow metallic waveguide [4]. Such fibers have previously been explored for their potential to suppress the losses and nonlinearities that inherently limit propagation within solid materials. Here, we address a different question, that of tailoring fiber *dispersion* for applications such as accurate dispersion compensation and dispersionless transmission. In contrast to previous work on dispersion control in Bragg and photonic-crystal fibers [5–10], we introduce a more general concept of designing dispersion via interactions between the core-guided modes and modes localized within intentional defects (*e.g.* Fabry-Perot cavities) in the multilayer cladding. In this way, we are not only able to obtain extremely large dispersion parameters, but we also benefit from a set of easily understood, independent "knobs" that one can adjust in order to tailor the functional form of the dispersion to suit particular needs. The strength of these knobs can also be interpreted as measures of performance degradation due to manufacturing inaccuracies. Moreover, unlike traditional silica fibers, in our fibers the intrinsic material dispersion is negligible, so the group-velocity dispersion is controlled entirely via tunable geometric parameters.

The multilayer cladding of the fiber in Fig. 1 has a photonic band gap that confines light in a certain frequency range determined by the periodicity. By changing the periodicity, or equivalently the overall scale to which the fiber is drawn, one can guide light at selectable wavelengths. Although the materials of the cladding may be highly lossy or nonlinear, these properties can be suppressed by many orders of magnitude for the core-guided modes, which have almost all of their fields within the hollow core. This permits a wide range of materials and wavelengths to be considered, including some that are not normally amenable to dielectric waveguiding [11–13]—and, in particular, one can choose high index-contrast chalcogenide/polymer combinations [12, 13] that lead to omnidirectional reflection. Omnidirectionality, while not strictly required for guidance, is strongly correlated with a metallic waveguide-like regime in which the light is almost entirely excluded from the cladding. In Section 2 we discuss the tools that we use for calculating the behavior of such fibers, and in Section 3 we analyze the behavior and theory of ordinary OmniGuide fibers.

Given any periodic photonic-crystal structure, one of the elemental building blocks for designing new behavior is the introduction of *defects* in the periodicity [14]. Such defects can confine localized modes whose frequencies lie within the bandgap, for example the familiar Fabry-Perot cavity mode [15] localized in an altered layer of a multilayer film (1d-periodic crystal). Another kind of defect is the termination of the crystal itself, which can give rise to surface states localized around the interface. We can create both sorts of localized defect modes in an OmniGuide fiber by altering one or more of the periodic cladding layers, as depicted by the second layer of Fig. 1(b). (Here, the layers are labeled "1," "2," *etc.* starting from the innermost layer, as shown in Fig. 2.) Because such a mode is separated from the core by a finite number of crystal layers, however, it can *interact* with the core-guided modes when their dispersion curves intersect, forming *anticrossings* that have predictably and radically altered dispersion. Section 3.2 discusses a simple model in which the qualitative behavior of anticrossings and their dispersion can be understood. This model allows us to define a set of "knobs" that in Section 4 we apply to design a dispersion-compensating fiber and in Section 5 to design two zero-dispersion transmission fibers.

#2267 - $15.00 US Received March 24, 2003; Revised April 25, 2003

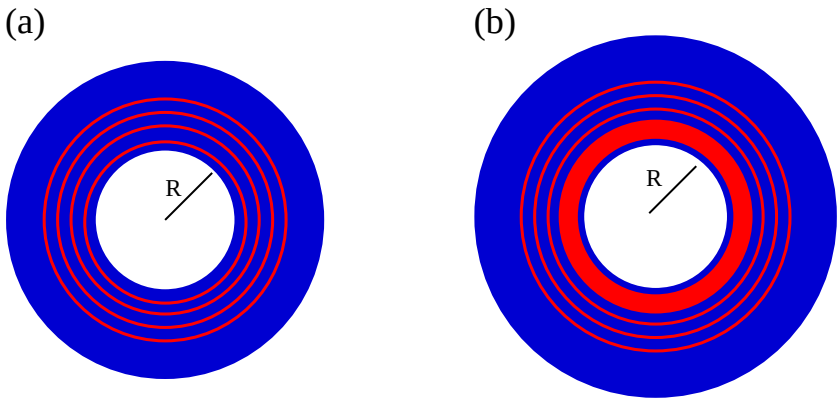

Fig. 1. (a) Defect-free OmniGuide fiber and (b) OmniGuide dispersion-compensating fiber. (Not to scale.) The defect-free ("long-haul") fiber consists of an air core (R=15.35 μm) surrounded by consecutive layers of refractive index=1.5 (blue) and refractive index=2.8 (red) materials. In this fiber, all the high-index layers have the same thickness (0.153 μm) and all the low-index layers have the same thickness (0.358 μm). The outermost region is a thick layer that provides structural stability. The actual number of layers used is larger than in this figure; in order to minimize radiation losses one would use 20 layers or more. The OmniGuide dispersion-compensating fiber is a modified structure that includes a defect, i.e. the thickness of one of the dielectric layers has been altered.

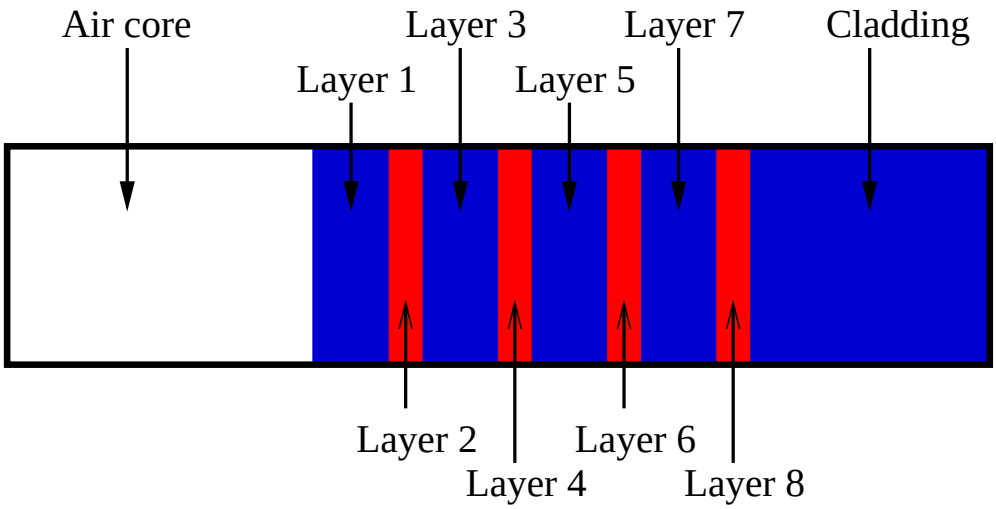

Fig. 2. Nomenclature: "Layer 1" denotes the material layer closest to the air core, the next-closest material layer is "layer 2," *etc.* "Core" means the air core inside the dielectric mirror and "cladding" means all layers outside the core. This figure is not drawn to scale and includes a reduced number of layers.

#2267 - $15.00 US
Received March 24, 2003; Revised April 25, 2003

1.2. Fiber dispersion

The chromatic (group-velocity) dispersion of a fiber is usually quantified in terms of the dispersion parameter D, which is defined from the dispersion relation as [16]

$$D = -\frac{2\pi c}{\lambda^2} \cdot \frac{d^2\beta}{d\omega^2}, \tag{1}$$

where c is the speed of light, λ the vacuum wavelength, ω the angular frequency, and β the wave number.

In the telecommunications field there is tremendous interest in dispersion and dispersion tailoring. A few years ago, the preferred strategy to avoid optical signal degradation due to chromatic dispersion was to minimize the dispersion parameter of transmission fibers, and thus fibers tailored to have zero dispersion at the operating wavelength—dispersion-shifted fibers—were invented [17]. Later, it was found that in order to suppress nonlinear effects such as four-wave mixing (FWM) in dense wavelength-division multiplexing (DWDM) systems, some dispersion was necessary; the point of zero dispersion was therefore shifted away from the operating wavelength. Such nonzero Dispersion-shifted fibers (NZDSF), which are widely used today, have a relatively low dispersion parameter whose value may strongly vary across the transmission band. Because the fibers have a non-zero dispersion, it becomes necessary to compensate the accumulated dispersion when transmitting over long distances or at high bit rates [16].

Dispersion compensation is usually accomplished through the use of dispersion-compensating fibers [18], which are fibers with a large, negative dispersion parameter. When a pulse that has been broadened due to propagation through a transmission fiber with a positive dispersion parameter passes through a fiber with negative dispersion, it can be compressed and regain much of its original shape. Absent other sources of signal degradation such as nonlinear effects, the pulse will fully recover its original shape when the length L and dispersion parameter D of the transmission fiber (t) and dispersion-compensating fiber (d) obey:

$$L_d \cdot D_d + L_t \cdot D_t = 0 \tag{2}$$

Creating a system where this equation is obeyed for a single wavelength is simple, as one can always choose a length of the dispersion-compensating fiber that will fulfill Eq. 2. However, accurately compensating the dispersion across a wide band is more challenging because D_t often varies significantly across the wavelength windows used in modern telecommunication systems, for instance varying from $\sim$3 to $\sim$6 ps/nm-km in Corning's E-LEAF fiber. To enable accurate dispersion compensation for multiple wavelengths, the *derivatives* of the dispersion parameter with respect to wavelength for the dispersion-compensating and transmission fibers must also match. Typically, higher-order derivatives of the dispersion parameter for transmission fibers are small, and therefore reduce this requirement to:

$$L_d \cdot \frac{\delta D_d}{\delta \lambda} + L_t \cdot \frac{\delta D_t}{\delta \lambda} = 0 \tag{3}$$

Combining Eqs. (2) and (3) enables the definition of a reduced dispersion slope R that must be the same for the transmission fiber and the dispersion-compensating fiber, if the dispersion-compensating fiber is to accurately compensate the dispersion of the transmission across a wide band:

$$R = \frac{1}{D} \cdot \frac{\delta D}{\delta \lambda} \tag{4}$$

To perform accurate dispersion compensation, it is consequently necessary to tailor the dispersion properties of the dispersion-compensating fibers to attain the proper reduced dispersion

#2267 - $15.00 US Received March 24, 2003; Revised April 25, 2003

slope. However, due to their small index contrast and simple geometrical structure, silica fibers offer limited opportunities for such tailoring. Bragg fibers, and especially those using a high index-contrast, offer much more room for dispersion tailoring and this has already been applied in several instances. Ferrando, Silvestre and Andrés [5] as well as Marcou, Brechet and Roy [6] showed that one could balance the waveguide dispersion and the material dispersion in a low index contrast Bragg fiber to create a fiber with zero dispersion over a wide wavelength range, which yields a fiber with interesting nonlinear properties. Recently Ouyang, Xu and Yariv [7] showed that by combining a high index contrast and a small core, one can attain a large, negative dispersion parameter. The literature also offers numerous examples of dispersion tailoring applied in the wider areas of photonic crystals [8] and photonic-crystal fibers [9].

Using defects to tailor the dispersion, as we propose to do in this work, is advantageous over applying a small core size as was done in [7] for several reasons. First, it enables a large dispersion parameter for a large-core fiber, thus reducing nonlinear effects. Furthermore, we can tailor the waveguide dispersion properties of the fiber at a much greater level of control, which both enables the creation of dispersion-compensating fibers with highly customized dispersion properties and opens up the possibility for other sorts of other dispersion tailoring, such as zero-dispersion and multiple-zero-dispersion transmission fibers.

2. Theoretical tools

The tools used in this work are the same as in [1], and are based on the transfer-matrix methods developed by [2]. For waveguides that lie along the z axis, we express the electromagnetic fields in the form:

$$\vec{F}(r)e^{i(\beta z-\omega t+m\phi)}, \tag{5}$$

where m is the angular-momentum "quantum number" and β is the (complex) wavenumber. We use Maxwell's equations to formulate the problem in terms of the longitudinal fields (E_z and H_z) for a given (m,β,ω). The fields in each layer are expanded in Bessel functions $J_m(k_j r)$ and $Y_m(k_j r)$ with $k_j \equiv \sqrt{n_j^2\omega^2/c^2-\beta^2}$:

$$\begin{aligned} H_z &= AJ+BY \\ E_z &= CJ+DY \end{aligned} \tag{6}$$

This yields a set of four coefficients (A, B, C and D) that describe the field in each layer. By matching the tangential field components across the boundaries between consecutive layers, we obtain a transfer matrix [2] that yields the coefficients in one layer as a function of the field in neighboring layers. The product of the transfer matrices for each layer yields a single 4×4 transfer matrix that relates the fields in the core to the fields in the outermost layer. By applying the boundary condition of zero incoming flux at the outermost layer [19], we obtain the eigenmodes of the system including both guided and leaky modes. The advantage of this approach over other methods often used to characterize optical fibers (for instance beam propagation methods or plane-wave based mode solvers [20]) is that the method exploits the cylindrical symmetry of the system to achieve high efficiency, making it easy to perform parameter exploration and optimization. The method has been verified to produce the same results for both the real and the imaginary part of β as more computationally demanding, generic methods. Combined with perturbation-theory techniques that are suitable for high-index contrast systems [21–23], the method is also an excellent starting point for describing systems that do not exhibit complete cylindrical symmetry [1].

#2267 - $15.00 US
Received March 24, 2003; Revised April 25, 2003

3. General principles

3.1. OmniGuide fiber without defects

In this section we will summarize the key features of the OmniGuide long-haul fiber (the defect-free fiber), which was introduced in Ref. [1]. This fiber consists of an air core surrounded by a cladding of consecutive layers of high and low index materials. The relative thickness of the layers is chosen according to the grazing-incidence quarter-wave condition [24]:

$$\frac{d_{hi}}{d_{lo}} = \frac{\sqrt{n_{lo}^2 - 1}}{\sqrt{n_{hi}^2 - 1}} \tag{7}$$

where d is the layer thickness, n is the index of refraction, and hi/lo signify high/low-index layer.

In [1], a system with indices of refraction of 1.6 and 4.6 along with an air core of index 1 was used, while we will here use indices of 2.8 and 1.5 since these indices correspond to more recent experimental systems [12, 13]. For these indices, Eq. 7 yields $d_{hi} = 0.30a$ and $d_{lo} = 0.70a$, where $a = d_{hi} + d_{lo}$ is the thickness of a bilayer. For the long-haul fiber, we use the high-index material in the odd-numbered layers, because the reflectivity of the dielectric mirror increases when the innermost layer is high-index.

Since Maxwell's equations are linear and scale-invariant, it is convenient to express all distances in units of a, all angular frequencies in units of $2\pi c/a$, and all wavenumbers in units of $2\pi/a$. Only when calculating physical quantities (such as the dispersion parameter D) is it necessary to match the parameter a to an absolute length scale. We choose the value of a so that the dielectric mirror provides maximum confinement for the central wavelength in the transmission band. For instance, if we want to transmit across the 40 nm C-band of long-haul telecommunication systems, we choose an a of 0.51 μm to provide maximum confinement around 1550 nm.

The band structure (dispersion relation) for the lowest-order modes of the OmniGuide Long-Haul fiber is illustrated in Fig. 3. In Fig. 3(a), we have plotted the edges of the transverse electric and magnetic band gaps together with the light line of air ($\omega = \beta c$), where we define TE/TM polarization as having electric/magnetic field in the plane transverse to the direction of propagation. Pure TM modes are confined by the TM band gap while pure TE modes are confined by the wider TE band gap. However, for modes with an angular quantum number larger than zero, the modes are hybridized with both TM and TE components. Therefore, the magnitude of the TM band gap determines the available bandwidth for transmission in these modes. Moreover, even for a pure TE mode, operation outside the TM gap may be problematic due to radiative coupling via fiber imperfections. When determining the available bandwidth, we thus consider the frequency range *along the light line* that is inside the TM band gap, since our operating mode is very close to the light line. Normally, when plotting a band diagram, one would just include the fiber bands in the figure that displays the band edges. However, because the large core places the bands of interest extremely close to the light line ($\beta = \omega/c$), we instead plot the bands separately in Fig. 3(b), where we plot the frequency (ω/c) *minus* wavenumber (β) as a function of wavenumber. The proximity to the light line can be appreciated by noticing that the scale on the y axis of this plot is two orders of magnitude smaller than the scale of the x axis.

The strong confinement in the fiber core, as illustrated by Fig. 4, makes it natural to label the modes in the diagram in analogy with metallic waveguides. In contrast, the near degeneracies in weakly guiding silica fibers that enable the "LP" mode labeling [25] do not apply to our fiber. Unlike the metallic nomenclature, we label $m \neq 0$ modes HE or EH instead of TE or

#2267 - $15.00 US Received March 24, 2003; Revised April 25, 2003

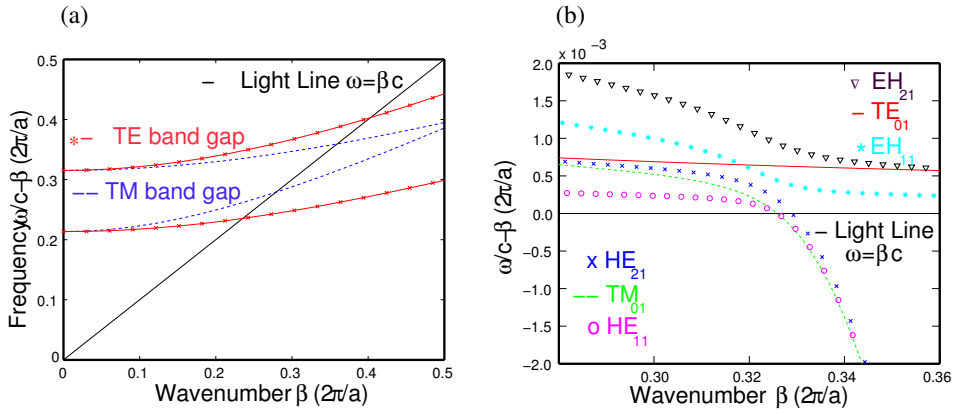

Fig. 3. (a) Band gaps and light line for OmniGuide long-haul fiber and (b) dispersion relations for the lowest-order modes.

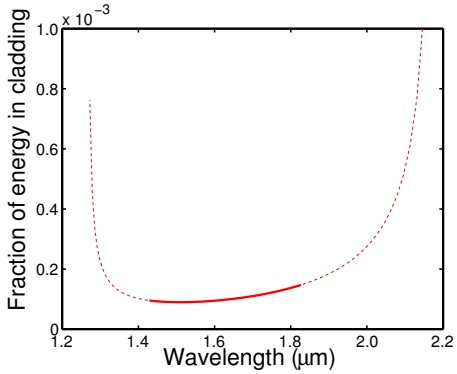

Fig. 4. Fraction of energy in the TE_{01} mode that is not confined in the core. The entire line shows the degree of confinement across the TE band gap, while the solid part of the curve indicate the part that is within the TM band gap (1430–1830nm) as well as the TE gap.

TM, since the higher order modes are not strictly transverse electric or magnetic due to finite penetration into the cladding. We apply the HE/EH label roughly according to whether the TE/TM component is dominant, as described in Reference [1]. For a more detailed discussion of the modal structure of the OmniGuide fiber, see Reference [26].

Just as in a metallic waveguide, the lowest-loss mode is the lowest-order, circularly-symmetric, "azimuthally polarized" TE_{01} mode. With only 17 layers (8.5 bilayers) surrounding the hollow core, the radiation losses of the TE_{01} mode becomes <0.001 dB/m! Due to its strong confinement in the core, the mode exhibits dramatic suppression of the nonlinearities and losses of the cladding material [1]. For instance, across the entire operating band, the absorption losses for the TE_{01} mode here are at least 40,000 times smaller than the bulk absorption losses of the materials. Thus, to limit the absorption losses to 0.01 dB/km, one can use materials with a bulk absorption of up to 400 dB/km, greatly expanding the material-design flexibility. Accessible materials include high-index chalcogenide glasses, which have recently been co-drawn in fibers together with polymers with a low index of refraction [12, 13]. Reference [13] demon-

#2267 - $15.00 US
Received March 24, 2003; Revised April 25, 2003

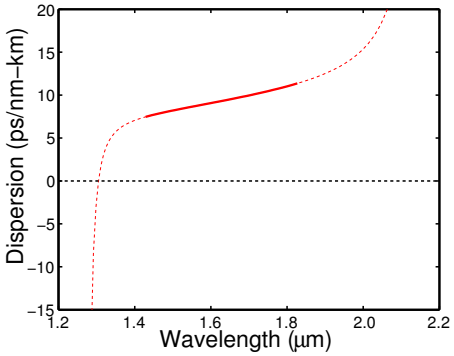

Fig. 5. Dispersion parameter for the TE_{01} mode in the OmniGuide long-haul fiber, where the solid part of the curve indicates the range that is within the TM band gap. Within the TM band gap the dispersion parameter D ranges from 7.5 to 11.4 ps/nm-km.

strates experimentally that OmniGuide fibers can suppress bulk absorption losses by up to four to five orders of magnitude at 10 μm, from bulk polymer losses of 10,000-100,000 dB/m to propagation losses of less than 1 dB/m.

The dispersion properties for the OmniGuide long-haul fiber over the wavelength range available for transmission can be found in Fig. 5, where we have plotted the waveguide dispersion as a function of wavelength. The strong concentration of the mode in the core explains why the material dispersion becomes negligible (less than 1% of the total). The figure illustrates that the fiber has dispersion values that are comparable to those of non-zero dispersion-shifted fibers (between 7.5 and 11.4 ps/nm-km within the TM gap), and that the dispersion slope is very low (averaging 0.01 ps/nm^2-km, which is an order of magnitude smaller than the slope of Corning's E-LEAF fiber).

The favorable performance parameters of the TE_{01} mode may be reduced by fiber imperfections (such as surface roughness, bends and ellipticity), which can cause coupling to more lossy modes. (Due to the large core and the high index contrast, the fiber supports a substantial number of higher-order modes.) Coupling to these higher order modes will not result in modal dispersion as it does for multimode silica fibers, however, since the higher-order modes have substantially higher losses than the TE_{01} mode, making the fiber effectively single mode, similar to what was observed in metallic waveguides. Nevertheless, mixing/leakage due to imperfections may become the dominant loss mechanism.

3.2. OmniGuide fiber with defects

The dispersion relation of the OmniGuide fiber can be significantly altered by introducing a geometric defect—a change in thickness of one (or more) cladding layers—into the otherwise periodic mirror structure. In this section, we introduce a simple model that can explain the qualitative effects of such defects.

The introduction of a geometrical defect leads to the formation of a "defect mode" similar to the situation in doped semiconductors. The energy of this mode is substantially localized within the defect itself, and its dispersion relation is situated inside the band gap, and a large portion of it is below the air light line. At points in the band diagram where the defect mode would intersect with a core mode of the same azimuthal symmetry ($\Delta m = 0$) and (for $m = 0$ modes) the same polarization, the defect mode may interact with the core mode. Thus, instead of the

#2267 - $15.00 US
Received March 24, 2003; Revised April 25, 2003

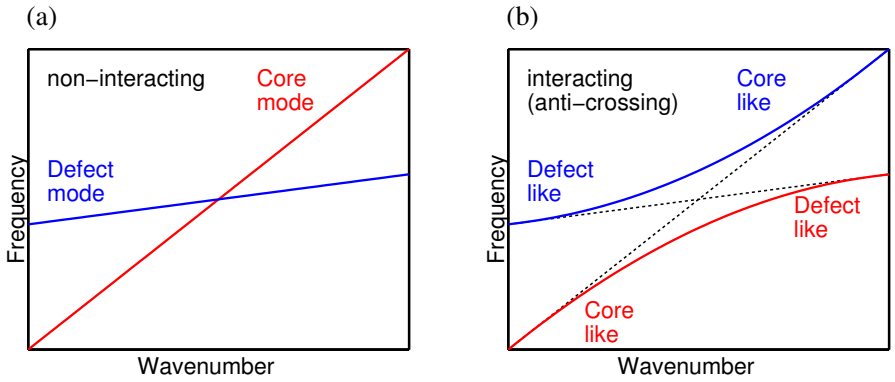

Fig. 6. Schematic representation of the effect of interaction between defect and core modes. Panel (a) shows the dispersion relations for the two modes without interaction and panel (b) shows how modal interaction changes the dispersion relations.

core mode and the defect mode crossing one another, the fiber mode will be "transformed" into a defect mode, and vice-versa, over a certain frequency range. Such band features are called "anticrossings" in solid-state physics [27]. In Fig. 6 we have made a schematic representation of this process. In Fig. 6(a) we see the dispersion curve for a core mode and a defect mode without interaction. The slope (group velocity) of the defect mode is much smaller than the slope of the core mode, because the group velocity for a mode localized in a medium of high refractive index ($v_g \sim c/n$) is much lower than for a mode localized in the core ($v_g \sim c$). This difference in group velocity makes the modes likely to intersect and implies a strong dispersion (rapid slope change) in the resulting anticrossing. Fig. 6(b) illustrates the effect of modal interaction, where the two modes no longer cross one another and instead the "core mode" changes its nature to become a "defect mode" and vice versa. In the transition region, the core mode radically changes its group velocity (approximately from c to c/n), which is synonymous with that mode having a large dispersion parameter in that frequency range. Figure 12(a) illustrates the transition from a core-confined to a defect-confined mode.

Quantitatively we can describe anticrossings in terms of coupled-mode theory [28, 29], whereby we can determine many features of the interaction by evaluating the coupling between the core and the defect modes, in direct parallel with the tight-banding approach in solid-state physics (see e.g. [27]). While such theory in principle can accurately describe the interactions of our system, it is in practice hard to make accurate predictions about dispersion values, because in our system it is unclear precisely what constitutes the "uncoupled" systems. Nevertheless, coupled-mode theory may be of great benefit for predicting *changes* in dispersion values due to modifications to the fiber structure and we will use it with modest success to predict the effect of changing the location of the defect layer.

The magnitude of the frequency range over which the transformation takes place depends on the strength of the interaction between the fiber mode and the defect mode, or in other words the degree of overlap between the fields of the two modes. If the interaction is weak, which will be the case if the defect is located far from the core, the frequency range over which the transition occurs will be narrow, resulting in sharp kinks in the dispersion relation for the given mode, as illustrated in Fig. 7(a). On the other hand, if the interaction is strong, the transition will take place over a broader frequency range and the kinks will be smoothed, as illustrated in Fig. 7(b). Since the dispersion parameter D is proportional to $\partial^2\omega/\partial\beta^2$, stronger interaction

#2267 - $15.00 US
Received March 24, 2003; Revised April 25, 2003

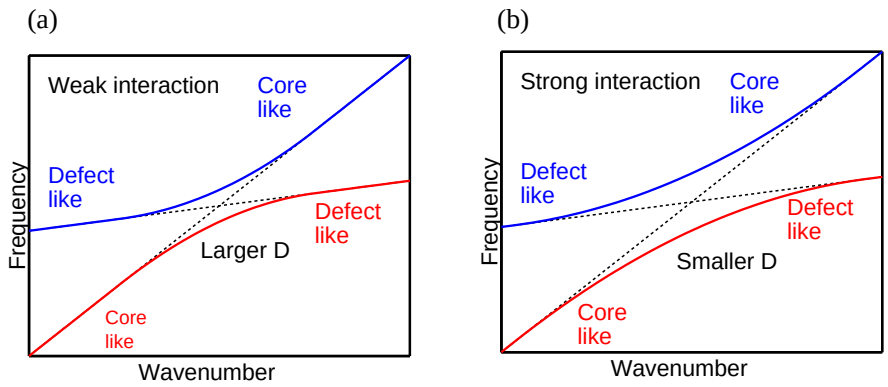

Fig. 7. Schematic representation of the effect of varying strengths of modal interaction. The modal interaction is weaker in panel (a) than in panel (b), resulting in a sharper "kink" in (a) and therefore a larger value of the dispersion parameter over a more narrow wavelength range.

translates into lower dispersion values.

Independent of the strength of the interaction, we find that the resulting product of dispersion parameter and wavelength range over which we achieve this dispersion parameter, i.e. the area A under the dispersion curve $D(\lambda)$ around the anticrossing, is only a function of the difference in $1/v_g$ between the core and the defect mode:

$$A = \int_1^2 D d\lambda = \int_1^2 \frac{\partial}{\partial \lambda}\left(\frac{1}{v_g}\right) d\lambda = \Delta\left(\frac{1}{v_g}\right) = \frac{1}{v_{g,1}} - \frac{1}{v_{g,2}} \tag{8}$$

This equation allows one to make simple predictions about the attainable dispersion characteristics. In our fiber, the anticrossing reduces the group velocity from c to $c/2.8$, which gives $A = 1.8/c = 6 \cdot 10^6$ (ps/nm-km)·(nm). For a wavelength range of 40 nm, the formula thus yields an average D of about 150,000 ps/nm-km. However, slope matching requirements, which we discuss later, reduce the usable area by a factor of 3-10, resulting in an average dispersion parameter of 15,000-45,000 ps/nm-km over a 40 nm band.

The frequency at which the modal interaction takes place depends strongly on the frequency range at which the defect mode itself exists. This frequency range, in turn, depends strongly on the size of the defect. Therefore, if we want to shift the frequency of modal interaction up or down, we can easily accomplish this by decreasing or increasing the size of the defect, respectively. Thus, we find that size and location of the defect provide us with two "knobs" that can be used to tailor the dispersion properties of the fiber in intuitively predictable ways.

Through the use of more complex defects, we can further modify the properties of the fiber. This could be accomplished by using multiple defects or by using a single defect that supports multiple defect modes. If we use a rather large defect, then this defect would support multiple modes and this would enable the interaction with the core-confined modes at multiple wavelengths. For the dispersion-compensating fibers presented in Section 4 we will mainly restrict ourselves to the use of a single, rather small defect, while we in Section 5 will demonstrate that the use of a defect that supports multiple modes can be used for creating a fiber with multiple points of zero dispersion.

The model for modal interactions presented here is only exact in the limit of weak interactions. For systems with stronger interactions between the modes it is imprecise to consider the

#2267 - $15.00 US
Received March 24, 2003; Revised April 25, 2003

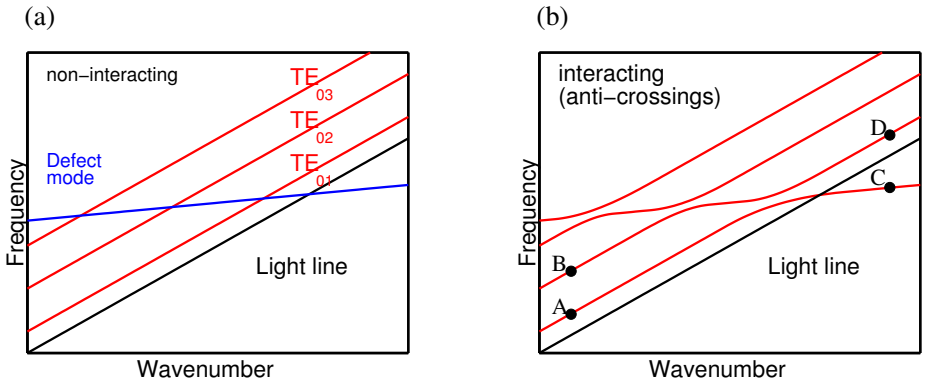

Fig. 8. Schematic representation of the interaction between a defect mode and multiple core modes. Panel (a) shows the defect mode (blue) and the core modes (red) separately, while panel (b) shows the resulting modal structure when the modes interact.

fiber and the defect as two separate systems whose resulting band diagram is the sum of the band diagram of the fiber and the defect separately. Furthermore, the simultaneous interaction between the defect and multiple bands may also alter the entire band diagram. So, the real band diagram for the fiber with a defect must be calculated using exact methods such as those described in Section 2. Nevertheless, the qualitative features of the anticrossing model remain.

So far, we have considered only the interaction of the defect mode with the lowest order core mode. In fact the defect mode alters the behavior of *all* modes that have the same azimuthal symmetry and polarization as the defect mode. In Fig. 8 we have illustrated this by plotting a more realistic picture of the band structure. In Fig. 8a we have schematically plotted the three lowest $m = 0$ modes (in red) together with one defect mode (in blue). For reference we have also included the light line in air ($\beta = \omega/c$), which illustrates that the defect mode is below the light line for a substantial part of its frequency range. In Fig. 8b, we see the effect of the interaction between the defect mode and the core-confined modes. For low frequencies, the three core-confined modes are all located above the light line and they strongly resemble the modes of the OmniGuide fiber without defects. As the frequency increases, the lowest $m = 0$ mode, the TE_{01} mode, starts interacting with the defect mode. The TE_{01} mode changes its character towards the defect mode (transforming from A to C). Around the same frequency the next lowest $m = 0$ mode, the TE_{02} mode, changes its character, and it starts to resemble the TE_{01} mode (transforming from B to D). For higher frequencies, the mode which at lower frequencies was almost identical to the TE_{02} mode is now almost completely identical to the TE_{01} mode of the defect-free OmniGuide fiber. We thus see that the defect mode can induce a transition from one core-confined mode to its neighboring core-confined mode. This change continues for all higher m=0 modes, and we therefore see that the presence of the defect makes all the core-confined modes take a “step down” around the frequencies where the defect mode crosses the dispersion curve of the core-confined modes. Transitions between core-confined modes can give large dispersion values useful for dispersion compensation. Such a mode has a frequency region of large negative dispersion followed by a region of large positive dispersion. This might be useful for certain dispersion-compensation schemes.

The model discussed above can also explain several interesting features of the defect-free OmniGuide fiber, whose dielectric mirror is perfectly periodic as in Fig. 1(a). For this structure, the termination of the periodic layers is itself a “defect” that can support a localized state,

#2267 - $15.00 US
Received March 24, 2003; Revised April 25, 2003

known as a surface state [14]. The interior surface of the OmniGuide long-haul fiber of Section 3.1 supports such a state and this can be seen in the dispersion relation of Fig. 3. For example, the HE_{11} mode undergoes an anticrossing similar to the lowest mode in Fig. 8, and therefore transitions to a surface state underneath the light line, while the EH_{11} mode undergoes a transition like the second-lowest mode in Fig. 8 to become HE_{11}-like. In this case, the states do not include an $m = 0$ TE mode, so the TE_{0l} modes are not affected. (This is because the "pure" defect mode of a flat surface would be a TM mode.)

The large dispersion parameters at the edges of the band in Fig. 5 for the TE_{01} mode of the OmniGuide long-haul fiber can also be understood in light of the anticrossing model. When the mode reaches the edges of the gap, there is an interaction with the continuum of cladding modes that leads to high dispersion. (This is only a rough picture, since the core/cladding modes do not remain weakly interacting.)

Examples of silica-based systems in which mode dispersion can be attributed to anticrossings include fiber Bragg gratings [30] (FBGs) and W-profile dispersion-compensating fibers [31]. In FBGs, the periodic index modulation (1D photonic crystal) creates a band gap via an anticrossing between forward and backward propagating modes at the Bragg wavelength, leading to strong dispersion effects. The strength of the interaction between the forward and backward propagating modes is determined by the strength of the index modulation, and stronger modulation gives lower dispersion over broader bandwidth, in accordance with Eq. 8. Exploiting the band-edge in FBG and similarly in etalons (thin-film filters) - often by putting multiple filters in sequence, enables very accurate dispersion control across a wide band. [32, 33]. So-called W-shaped DCFs have a W-formed index profile: a high-index core is surrounded by a low-index ring, and outside of this ring there is another ring of high index, which is finally surrounded by a low-index cladding. Thus, light can be index-guided in either the high-index core or the high-index ring. Due to the different effective indices in the core and in the high-index ring, modes confined in those two regions core will have different group velocities. Due to interaction between the modes, the anticrossing creates a mode which transforms itself from being confined in the core to being confined in the high-index ring over a certain frequency range, and in this transition region the mode exhibits a very large dispersion; and this has been demonstrated both theoretically [31] (-5100 ps/nm-km) and experimentally [34] (-1800 ps/nm-km). However, because the difference in effective index between the high-index core and the high-index ring is at most on the order of a few percent, the dispersion parameter will be much lower than in an OmniGuide dispersion-compensating fiber.

4. Design of dispersion-compensating fibers

Having concluded on general principles that the OmniGuide fiber structure offers an opportunity to obtain a large dispersion parameter, we turn to the design of an actual dispersion-compensating fiber. In Section 4.1 we demonstrate that we can use this structure to create a fiber with remarkable dispersion magnitudes and show how to tailor the dispersion. In Section 4.2, we discuss the important issue of coupling between this dispersion-compensating fiber and silica-based transmission fibers. In Section 4.3 we consider the impact of material parameters on the performance of the fiber.

4.1. Optimizing performance parameters

When tailoring the dispersion properties of the fiber, we mainly make use of three "knobs:" the location of the defect, the size of the defect, and the overall scaling of the structure.

The significance of the location of the defect can easily be understood by analyzing the defect-core interaction model with coupled-mode theory. If, using Dirac notation, we describe the operating mode (field pattern) of the defect-free fiber as $|\psi_1\rangle$ and of the defect mode as $|\psi_2\rangle$,

#2267 - $15.00 US Received March 24, 2003; Revised April 25, 2003

then by substituting $\pm$ (bonding/antibonding) combinations of these states into the variational theorem (or, equivalently, using first-order perturbation/coupled-mode theory), one finds that the frequency splitting is proportional to the inner product:

$$\Delta\omega \sim \Re\left\langle \psi_1 \middle| \hat{H} \middle| \psi_2 \right\rangle \tag{9}$$

where $\hat{H}$ is a coupling operator (the "Hamiltonian" operator of the combined system). This inner product has two main contributions, from the exponential tail of $|\psi_1\rangle$ in the defect (peak of $|\psi_2\rangle$) and vice versa.

Calculations show that in the dielectric mirror, the field decays by approximately a factor of three for each bilayer. Therefore, the contribution to the split from each of the two terms mentioned above should decay by approximately a factor of three if we separate the defect and the core by an additional bilayer. However, the sum of these two terms will not necessarily decay by exactly a factor of three, because the relative phase of these two terms can change; this will induce an oscillation in addition to the overall exponential decay of the splitting, as seen below.

It then follows that the increased dispersion at the anticrossing is inversely proportional to $\Delta\omega$, and thus increases exponentially (plus some oscillation) with the depth of the defect as seen in table 4.1. This is due to the fact that the $\Delta\beta$ width of the anticrossing region is proportional to $\Delta\omega$, combined with Eq. 8.

In Figs. 9(a) and (b) we show exact calculations of the dispersion relation and the dispersion parameter as a function of wavelength for four different locations of the defect: the second, fourth, sixth, or eighth layer. In all cases, we create the defect by making one high-index layer twice as thick as all the other high-index layers. The thicknesses of all remaining layers are chosen according to the grazing-incidence quarter-wave condition of Eq. 7, such that all remaining high-index layers have the same thickness and all low-index layers have the same thickness. Since an even-numbered layer has the high-index value, the innermost layer here is low-index. In Fig. 9(a), we have indicated the point of minimum dispersion parameter for each of the dispersion curves from Fig. 9(b) with a dot.

Table 1. The dispersion increase at an anticrossing is roughly proportional to the amplitude of the exponential field tails as a function of defect location, causing the product of the two to be roughly constant (with some oscillation).

Defect layer	2	4	6	8	10	12
Max field (arb. units)	0.51	0.22	0.092	0.039	0.017	0.0070
D (ps/nm-km)	-45,000	-51,100	-159,000	-511,000	-1.45M	-2.14M
D ·max field (arb. units)	23,000	11,000	15,000	20,000	23,000	15,000

Furthermore, the plots reveal that we can obtain extremely large dispersion parameters, around -500,000 ps/nm-km, by placing the defect in the eighth innermost layer. These values are more than three orders of magnitude larger than the dispersion parameter of contemporary dispersion-compensating fibers and four to five orders of magnitude larger than the dispersion in most transmission fibers. Thus, the dispersion accumulated from the propagation through 10 km of transmission fiber can be compensated by propagation through approximately 1 meter of these dispersion-compensating fibers. Because the values we attain for the waveguide (geometric) dispersion are so large, we need not consider the small contribution from material dispersion. Fig. 9(a) also shows that the point of minimum dispersion parameter for all four curves is below the light line (ω/c=β). We will further discuss the consequences of the mode being below the light line in Sec. 4.2 and 4.3.

#2267 - $15.00 US Received March 24, 2003; Revised April 25, 2003

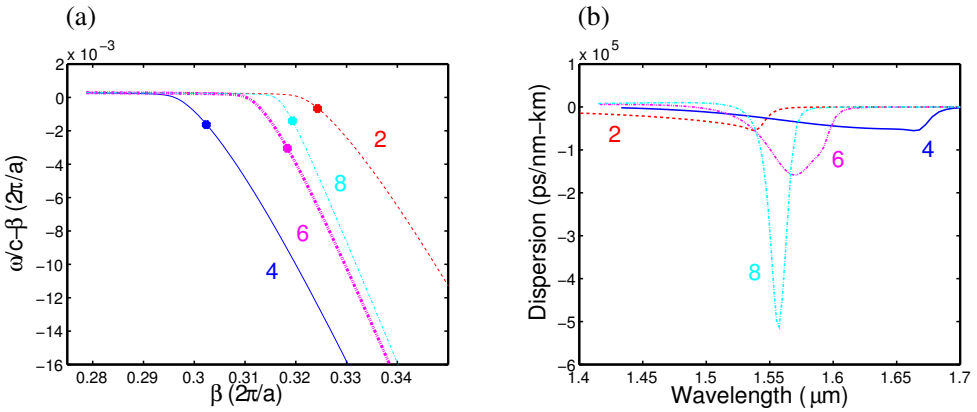

Fig. 9. Dispersion relation (a) and dispersion curve (b) for four different locations of the defect. Both curves show that the transition from core-confined mode to the defect mode takes place more rapidly when the defect is located far from the core which results in a large negative dispersion parameter over a narrower band. The point of minimum dispersion parameter is indicated with a dot on the dispersion relations.

By locating the defect deeper in the mirror, we obtain a higher dispersion parameter value over a narrower band. Consequently, the slope of the dispersion curve is also greater the deeper we bury the defect. Thus, when choosing how far away from the core to place the defect, we do so to ensure that the reduced dispersion slope approximately corresponds to the slope of the transmission fibers whose dispersion we want to compensate. If we, for instance, want to compensate the dispersion of Corning's E-LEAF fiber, whose dispersion slope makes the dispersion parameter double across the 40 nm C-band, we choose to locate the defect in the fourth layer from the core. With the defect in this layer, the slope of our fiber corresponds fairly well with the slope of the E-LEAF fiber over a wavelength range well in excess of the C-band.

In order to fine-tune the performance of the fiber, we turn to the second knob we have at our disposal: the size of the defect. The purpose of this fine tuning is to ensure that the reduced dispersion slope of the dispersion curve accurately matches the slope of the target transmission fiber. For instance, upon inspection of the dispersion curve for the structure with its defect in the fourth layer in Figure 10, we find that the reduced dispersion slope of the OmniGuide dispersion-compensating fiber at 1530 nm matches the reduced dispersion slope of Corning's E-LEAF fiber at 1550 nm. We would thus like to "move" the dispersion curve for this fiber by 20 nm. By coupled-mode theory, we would thus like to increase the the resonance wavelength of the defect mode by approximately 1.5%. If we assume the resonance mode of the defect is the lowest mode of the defect and model it as a Fabry-Perot cavity surrounded by metallic walls, simple analysis shows that we can increase the resonance wavelength by 1.5% by increasing the width of the cavity by 1.5%, and we indeed find that such an increase in the width gives the predicted effect, as illustrated in Fig. 10. Having tuned the thickness of the defect layer, we obtain a fiber whose slope matches the slope of Corning's E-LEAF fiber to a precision that exceeds the variations in the slope due to fiber manufacturing inaccuracies and seasonal variations in temperature [35].

This sensitivity to small changes in the thickness of the defect layer can place high demands on manufacturing tolerances, which could result in low production yields. We can address this problem by exploiting a third knob, namely the possibility of varying the thickness of all layers

#2267 - $15.00 US
Received March 24, 2003; Revised April 25, 2003

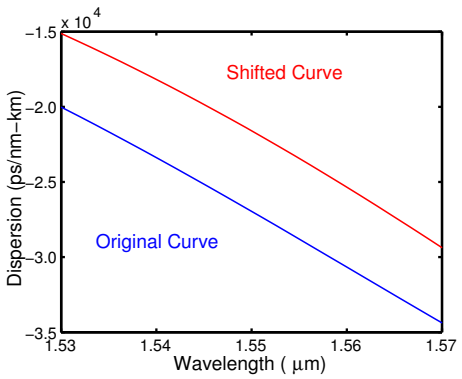

Fig. 10. Dispersion curve for two slightly different sizes of the defect. The defect for the red curve is 1.5% larger than the defect for the blue curve.

via overall scaling, controlled via the fiber drawing speed. Because of the sensitivity of dispersion properties for photonic-band-gap fiber with defects to variations in layer thickness, the needed rescaling would be very small, and we would therefore not expect significant degradation of any specifications for the outer diameter.

The effect of rescaling the fiber dimensions is to change the scaling parameter a, which shifts the entire dispersion curve proportionally to the change in a. For instance, an increase in dimensions by 1% will translate the dispersion curve by 15 nm towards the longer wavelengths and therefore decreases the reduced dispersion slope in the region where the dispersion slope is negative. In addition to translating the dispersion curve (changing the x-scale of Fig. 10), a change in a also changes the y-scale of the dispersion curve: the value of the maximum dispersion parameter changes inversely with the change in a.

We can also change the thicknesses of multiple dielectric layers independently, for instance if further fine-tuning of the dispersion properties is desired. The use of multiple defects could create multiple regions of high dispersion, and by exploiting multiple defects these regions can be placed at arbitrary frequencies relative to one another. Using a single, large defect would create multiple regions of high dispersion with a nearly fixed frequency spacing between them. We do not, however, exploit the simultaneous use of multiple defects in this paper.

Finally, we can also alter many properties of the fiber by changing the size of the core. We find that the dispersion properties of the fiber remain surprisingly constant with core diameter, however, in the regime of interest for us (negative dispersion slope). This is because the contribution to the dispersion from the core size is $D_{core} \sim 1/R^2$ [1], so only for very small values of R does this become significant. This mechanism explains the large dispersion in small core-size fibers observed by Ouyang *et al.* [7].

To give a specific example of the effects of core size in OmniGuide fibers with defects, Fig.11 shows the dispersion curve for two fibers whose only difference is that one has a core radius of 14.8 μm while the other's core is six times smaller, $R = 2.47\ \mu m$. The properties that are most strongly affected by changing the core area are the nonlinearities and intermodal coupling by fiber imperfections. As we reduce the core area, the effective modal area is reduced, which increases any nonlinear effects. Because the defect mode is mainly located around the ring defined by the defect, we find that the modal area is *linearly* proportional to the core radius (and not proportional to the square, as it is for core modes).

#2267 - $15.00 US
Received March 24, 2003; Revised April 25, 2003

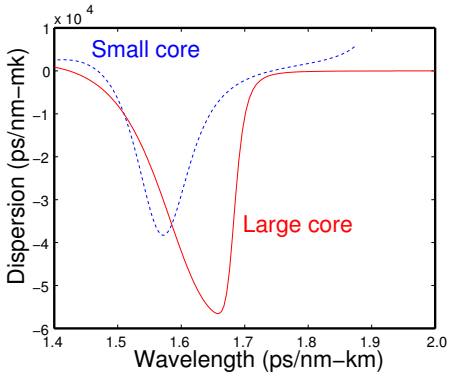

Fig. 11. Dispersion curve for two different core sizes, the large core (red) having a core radius of 14.8 μm and the small core (blue) having a radius of 2.98 μm.

4.2. Coupling

In order to induce a dispersion that is three orders of magnitude larger than the dispersion of silica-based dispersion-compensating fibers, we change the nature of the operating mode radically across the band where the mode is confined. At the lowest frequency (longest wavelength) the mode resembles the operating mode of an OmniGuide long-haul fiber, a metallic-like TE_{01} mode which in our dispersion-compensating fiber has more than 99.5% of its power in the core. This mode is located above the light line, and thus the confinement of this mode is entirely provided by the photonic band gap of the dielectric mirror surrounding the air core. At the higher frequency, which is where we in fact operate the fiber to obtain dispersion-slope matching, the mode profile is radically different, with most of the power located in the vicinity of the defect layer. The mode is located well below the light line and therefore is confined relative to the air core by index guiding. In the outer direction the field is still confined by the photonic band gap. This mode is therefore a good example of a surface state [14]. The difference in modal profile is illustrated in Figure 12 where we see the modal fields at a low frequency (corresponding to a wavelength of 1.75 μm) and at a higher frequency (corresponding to a wavelength of 1.55 μm). These frequencies lie at either side of the frequency region where the anticrossing occurs.

The operating mode has a profile very dissimilar from that of any transmission fiber, so it is nearly impossible to couple directly between the two. In order to obtain efficient coupling, one may introduce an initial taper in the disperson-compensation fiber (a common technique for coupling to modes with unusual profiles [36]). By decreasing all the dimensions of the fiber by approximately 13%, the field profile of the operating mode will resemble the TE_{01} mode of the OmniGuide long-haul fiber. We can thereby couple directly to a tapered version of the dispersion-compensating fiber from the OmniGuide long-haul fiber to compensate dispersion accumulated in the latter.

If one wants to compensate the dispersion accumulated in contemporary silica transmission fibers, it is also necessary to convert the linearly polarized operating mode of single-mode silica fibers (the LP_{01} mode) into the TE_{01} mode. This can be accomplished, for example, by two steps. First, one butt-couples from silica fibers into the HE_{11} mode of the OmniGuide fiber, a process which is simple due to the strong similarity between the HE_{11} of OmniGuide's fibers and the LP_{01} mode of silica fibers. Second, one can convert from the HE_{11} to the TE_{01} mode using a bend converter [37], a process that can yield more than 90% coupling efficiency [38] for one of the LP_{01} polarizations.

#2267 - $15.00 US
Received March 24, 2003; Revised April 25, 2003

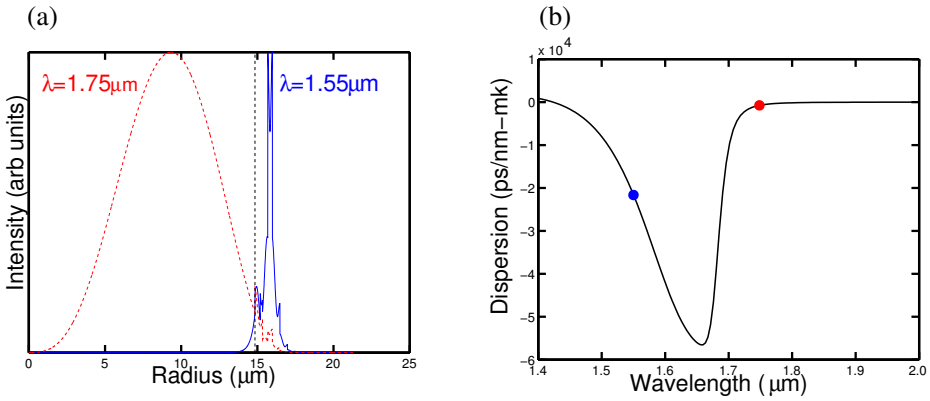

Fig. 12. Panel (a) shows the energy density of the operating mode as a function of distance from core center at two different wavelengths. The solid (blue) line represents the energy distribution at 1.55 μm, which is in the center of the operating band and the dotted (red) line represents a wavelength on the other side of the anticrossing. The vertical black line represents the core radius. Panel (b) shows the dispersion curve with dots signaling the two wavelengths for which the energy distributions can be found in panel 9a).

4.3. Discussion

The fact that a large part of the power in the operating mode is localized in the defect for the wavelengths of interest means that the operating mode in the dispersion-compensating fiber will "see" more of the properties of the materials in the dielectric mirrors than the operating mode of the long-haul fiber does. Therefore, the performance of the fiber (such as the figure of merit, defined as dispersion parameter divided by losses per unit length) of this fiber will be affected much more by material parameters than is the case for the defect-free fiber. Because some possible high-index material candidates have quite high absorption losses and nonlinearities, the resulting fiber losses and nonlinearities experienced per unit length of fiber will be larger than for silica-based dispersion-compensating fibers. However, since the dispersion parameter of the OmniGuide dispersion-compensating fiber is approximately three orders of magnitude larger than those of silica based dispersion-compensating fibers, we can tolerate losses per unit length that are much higher than in such fibers.

To make specific predictions about the loss and nonlinear performance, we need to make assumptions about the inherent material properties. Chalcogenide glasses, an attractive high-index material, have losses ranging from $\sim$100 dB/km to thousands of dB/km [39], therefore a loss of 400 400 dB/km seems realistic. If one uses silica glass as the low-index material, its contributions to the absorption losses will be negligible. Using these numbers we will now calculate the figure of merit; we employ a fiber structure with a defect in the fourth innermost layer that is twice the thickness of an ordinary high-index layer, but rescale the entire structure (ie, change the dimension of the scaling parameter *a*) so that the operating wavelength (1.55 μm) is at the point of maximum negative dispersion parameter *D*. At this point, *D*=-54,200 ps/nm-km and the material absorption is 45 dB/km, giving a figure of merit of 1200 ps/nm-dB. The large absorption losses reflect the fact that in this dispersion-compensating fiber the operating mode has a substantial presence in the defect. Alternatively, if we operate the fiber in the region where its slope is matched with Corning's LEAF fiber, we obtain a figure of merit of 246 ps/nm-dB (the figure of merit *across a band*, here 40 nm, is defined as the maximum dis-

#2267 - $15.00 US
Received March 24, 2003; Revised April 25, 2003

persion divided by maximum losses). If one could reduce bulk absorption losses to 100 dB/km (for instance through more careful selection of high-index material and better materials processing), the FOM would increase to 984 dB/nm-dB. For comparison, commercially available dispersion-compensating fiber modules have figures of merit ranging from 50 to 200 ps/nm-dB.

In the calculations above, we assumed that there were no contributions to losses due to radiation, even though for a finite number of layers some power will leak out. However, for the dispersion-compensating fiber design we find that at 1.55 μm adding a single bilayer will decrease the losses by a factor six, and one can therefore achieve arbitrarily low radiation losses by using a sufficiently large number of layers. Using only thirty layers we obtain losses that are below 1 dB/km, which is so far below the absorption losses that the losses due to radiation are negligible.

5. Design of zero-dispersion transmission fibers

Thus far in this work, we have focused on exploiting the flexibility of the OmniGuide fiber structure to create a fiber that can compensate the dispersion accumulated in transmission fibers. A more appealing way of addressing the problem of dispersion than the addition of dispersion-compensating devices to transmission systems would be to eliminate the dispersion in the transmission fibers themselves. This strategy has been widely employed using the Zero Dispersion Shifted Fibers. These are single-mode silica-based transmission fibers whose index profile has been tailored such that the waveguide dispersion and material dispersion balance each others exactly. However using such fibers in DWDM systems was problematic, because zero dispersion enhances interchannel nonlinear effects such as four-wave mixing. Therefore, to avoid the nonlinear effects in silica fibers, modern transmission systems employ fibers with a small, positive dispersion parameter, which necessitates dispersion compensation.

The OmniGuide fiber structure offers a different and far more appealing solution to the problem: the OmniGuide transmission fibers have nonlinearities that are four orders of magnitude lower than those of silica fiber, and therefore operating the fiber at or near zero dispersion is feasible, even for multichannel systems with low channel spacing. Unfortunately, the OmniGuide long-haul fiber does have a positive dispersion parameter on the order of 7-10 ps/nm-km, as Fig. 5 shows. It would therefore be beneficial to modify the design of this fiber to achieve zero dispersion. We do this by changing the thickness of a few of the innermost layers so as to allow some power to penetrate into the cladding, like in the dispersion-compensating fiber. The resulting structure is equal to the structure of the long-haul fiber, except that the odd numbered layers have low index, layer 1 has thickness 0.256 μm (instead of 0.358 μm) and layer 2 has thickness 0.137 μm (instead of 0.153 μm). All layers outside these two innermost layers have the same dimensions as the long-haul fiber, as governed by the grazing-incidence quarter-wave condition of Eq. 7. However, we choose to operate this fiber at the wavelength of zero dispersion. At this wavelength, less than 0.1% of the power penetrates into the cladding, and therefore the losses and nonlinearities of the cladding materials remain strongly suppressed. Absorption losses will only be an order of magnitude larger than for the long-haul fiber, and because the nonlinearities of the fiber are still governed by the nonlinear coefficient of the air core, the nonlinearity of this fiber will only increase by a few percent. For power levels used in modern communication systems, we therefore do not expect nonlinear effects to play any significant role.

Although the underlying reason for the modified dispersion behavior in this situation is the same as in the dispersion-compensating fiber design, its manifestation is quite different, in particular the dispersion parameter is shifted marginally (compared to the changes in the dispersion-compensating fiber). The difference is due to the much stronger interaction between the core and cladding mode, which causes a much more gradual transition to the defect state. The interaction is strong because the defect is in the two layers closest to the core. Furthermore

#2267 - $15.00 US Received March 24, 2003; Revised April 25, 2003

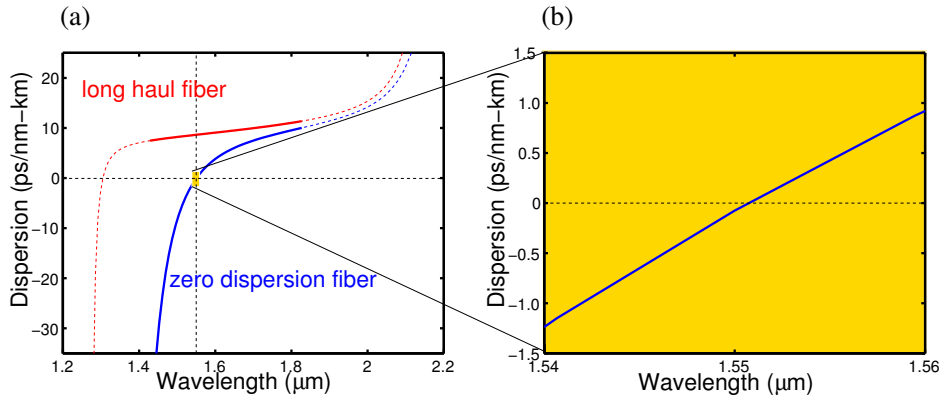

Fig. 13. Dispersion curves for OmniGuide zero dispersion fiber. Panel (a) shows the dispersion of the zero dispersion fiber together with the OmniGuide long haul fiber over a broad wavelength range. Panel (b) zooms in on the dispersion properties for the zero dispersion fiber over a 20 nm band.

the frequency of strongest interaction between the defect mode and the operating mode is far from the operating wavelength, and this reduces the effect of the defect further. The overall result is thus a mode which strongly resembles the core mode of a defect-free structure, but with slightly modified dispersion characteristics.

Achieving zero dispersion at a single wavelength is of little value if the dispersion slope around that point is large. We therefore design the Zero Dispersion fiber to have as flat a dispersion slope as possible. The resulting dispersion curve can be found in Fig. 13. This curve has a dispersion slope of 0.11 ps/nm^2-km. Using a dispersion limit of [16]

$$B^2 \cdot D \cdot L < 2 \cdot 10^5 \tag{10}$$

we can estimate the information carrying capacity as a function of fiber length for uncompensated transmission. We find that the Zero Dispersion Fiber can support 25 40 Gb/s channels over a distance of 100 km, or it can alternatively support 200 10 Gb/s channels over 500 km. We have here used a channel spacing of 100 GHz for the 40 Gb/s signal and 50 GHz for a 10 Gb/s signal. These are conservative estimates for the required channel spacing, since the low nonlinearities permit the use of modulation formats that minimize the spectral width of the signal.

As a more exotic example of the principle of tailoring dispersion properties by introducing a defect, we show that by creating a fiber with a large defect we attain *multiple* points of zero dispersion. This can be accomplished by making the defect so large that it supports multiple modes, as illustrated in Fig. 14. We see that between the regions of strong interaction between the core and cladding mode, there are regions where the second derivative of the frequency changes sign, and hence these will be points of zero dispersion. By making layer 1 a low-index layer 9.9 μm thick and using the regular structure defined by the quarter wave condition of Eq. 7 outside this layer we obtain a defect that supports so many $m = 0$ defect modes within the TE band gap that the fiber has eight points of zero dispersion, as Fig.15 illustrates.

An important advantage of this fiber over other zero dispersion fibers, which further immunizes the fiber against nonlinear effects, is that the different points of zero dispersion in fact have different group velocities. Therefore, if we would choose to operate one channel at each point of zero dispersion, these different channels would not interact with each other with the

#2267 - $15.00 US
Received March 24, 2003; Revised April 25, 2003

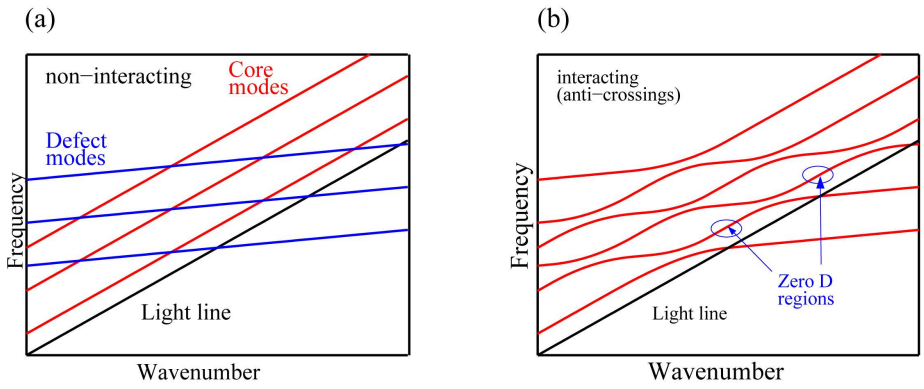

Fig. 14. Schematic representation of the interaction between multiple defect modes and multiple core-confined modes.Panel (a) shows three defect modes (blue) and the core-confined modes (red) separately, while panel (b) shows the resulting modal structure when the modes interact.

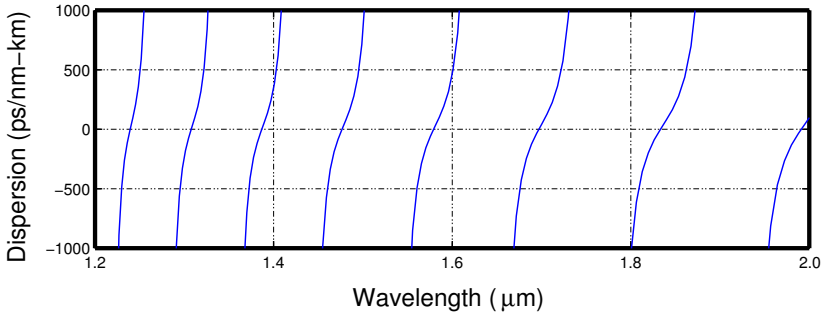

Fig. 15. Dispersion curve for the OmniGuide multiple zero dispersion fiber.

strength of neighboring channels at zero dispersion; in fact, the phase matching between the different channels corresponds to that of a fiber with an extremely large dispersion parameter. Thus, the difference in group velocity effectively prevents four wave mixing, whereas the low nonlinearities of the core as well as the zero dispersion prevent problems due to self phase modulation. Consequently the fiber provides good protection against all types of Kerr nonlinearities. Unfortunately, the large dispersion slope ($>$15 ps/nm^2-km at the point of zero dispersion) of the fiber significantly limits the amount of bandwidth each zero-dispersion point could support. Applying the same parameters as we did in the section on the Zero Dispersion Fiber, we find that each point of zero dispersion could support one 10 Gb/s channel over 500 km.

6. Conclusions

We have shown that the group-velocity dispersion of photonic bandgap fiber can be tailored by introduction of geometrical defects in the otherwise perfectly periodic structure that guides light within the fiber core. We presented several examples of such tailoring that attain unprecedented dispersion characteristics, by using exact theoretical methods. Moreover, we have introduced a powerful theoretical model, based on a “tight-binding” picture of core/defect mode anticross-

#2267 - $15.00 US
Received March 24, 2003; Revised April 25, 2003

ings, which provides a basis for understanding and designing the dispersion behavior of a wide range of physical systems.

In the model system of a hollow-core OmniGuide fiber, which guides light within Bragg mirrors formed by concentric rings of two alternating dielectrics, we have demonstrated several unusual results. First, we designed a dispersion-compensating fiber that attains dispersion parameters of up to -500,000 ps/nm-km with the ability to match the dispersion slope of an arbitrary transmission fiber. Such a large dispersion parameter enables dispersion compensation in 1/1000 the length of conventional compensating fibers. Moreover, the dispersion/loss figure of merit exceeds that of contemporary systems by up to a factor of 5; even better values could be obtained with future material developments for photonic bandgap fibers. Second, we designed a transmission fiber with a range of near-zero dispersion sufficient to transmit 200 10 Gb/s channels over 100 km without requiring compensation. Moreover, this fiber design exploits the ability of hollow-core OmniGuide fibers to suppress material nonlinearity, to such an extent that nonlinear effects such as four-wave mixing are negligible over the above-mentioned transmission span. Third, we exploited the simple design principles provided by our anticrossing model in order to demonstrate a fiber with multiple frequencies having zero dispersion, providing an interesting medium for wavelength-multiplexed transmission.

We present the above designs within the theoretical framework of a simple model involving the interaction between the conventional core-guided mode and a "defect mode" confined by an intentional defect introduced in the periodic photonic-crystal cladding. As viewed in a coupled-mode (or tight-binding) framework, when the dispersion relations of these modes intersect they interact to form an anticrossing region, characterized by a sharp exchange in mode slope and field pattern between the two modes. If the modes are weakly interacting (well separated), this results in high dispersion, and in other cases one can obtain unusual tailored dispersion characteristics. Not only does this model provide an intuitive understanding of the modal characteristics obtained by an exact calculation, but it also makes clear the influence of different structural parameters ("knobs") that can be used to tune the dispersion. Furthermore, these basic principles can also be applied to enhance the understanding of many other technologies employed in contemporary transmission systems, including fiber Bragg gratings, etalons, and W-shaped dispersion-compensating fibers.

Because our anticrossing picture expresses the fiber behavior as a composite of two much-simpler waveguides that are already well understood, one can find a set of independent knobs that control one waveguide at a time or the interaction of the two. The first knob is the depth of the defect within the cladding, which controls the interaction strength: the interaction decreases exponentially, with a corresponding increase in dispersion, with the depth, as can be seen from coupled-mode theory. The second knob is the structure of the defect, and in particular the size of the defect layer: this shifts the frequency of the defect mode (and thus the anticrossing) up and down proportionally to the size as understood by Fabry-Perot cavity theory. As is also well understood from the Fabry-Perot theory, a sufficiently large defect will support multiple defect modes, leading to multiple anticrossing, which we exploited to obtain multiple dispersion zeroes. A third knob is the overall scaling of the structure, which by the scalability of Maxwell's equations leads simply to a scaling of the wavelengths and field patterns. This knob is particularly useful because it can be controlled dynamically during fiber drawing to fine-tune dispersion slope and other characteristics. Finally, an understanding of these knobs not only permits design and tuning of the dispersion; it also determines the corresponding manufacturing tolerances.

#2267 - $15.00 US Received March 24, 2003; Revised April 25, 2003